Low-temperature alteration and magnetic changes of variably altered pillow basalts

Daming Wang, Rob Van der Voo and Donald R. Peacor

Department of Geological Sciences, University of Michigan, Ann Arbor, MI 48109-1063, USA. E-mail: voo@umich.edu

SUMMARY

Pillow basalt fragments from the East Pacific Rise, dredged during the Phoenix expedition, often show discoloured rims due to alteration. A suite of nine pillow basalts with such discoloured rims and ranging in age between 200 and 820 ka has been characterized in terms of their Fe–Ti-oxide mineralogy and rock magnetic properties. These large pillow fragments show relatively unaltered grey interiors, surrounded by darker, concentric halos, which vary in thickness as measured from glassy pillow rims and surfaces caused by large cracks penetrating into the original pillow interior. The discoloured zones are characterized by precipitation of abundant secondary minerals, such as Fe^{3+}-rich clays that filled vesicle spaces. Fe–Ti oxides in subsamples from discoloured rims and grey interiors have been investigated with electron microscopy and rock magnetic techniques. The subsamples come from traverses that are parallel to the outer glassy pillow rims, allowing us to study the low-temperature alteration effects and rock magnetic properties without having to take variable grain size into account.

Not surprisingly, titanomaghemites in discoloured rims are, in a general sense, oxidized to a higher degree (z typically >0.55) than those in the relatively unaltered grey interior (z typically <0.55). However, exceptions are numerous and reveal that oxidation state of the Fe–Ti oxides and visible alteration in the discoloured rims are not directly correlated. Moreover, the alteration front of the discoloured rims does not generally coincide with a pronounced jump in z. The titanomaghemite within the discoloured rims appears to have oxidized relatively quickly, reaching $z > 0.6$ within 200 000 yr. The difference between the oxidation states of titanomaghemite within the grey pillow interior and the discoloured rims gradually diminishes with increasing age, so that for samples with ages of 800 ka the oxidation state of titanomaghemites in the grey interior approaches that of the discoloured rim.

Our study demonstrates that visible discolouration of pillow basalts is not a suitable proxy for z. Because average Ti content can vary from sample to sample, Curie temperatures are also inaccurate proxies for z. If one wants to study possible correlations between z and rock magnetic parameters, the best technique is to determine z for each subsample by using transmission electron microscopy (TEM), electron microprobe, Mössbauer or similar techniques. In agreement with many (but not all) previous observations on natural samples, we find that bulk coercivity (H_c), and high-field susceptibility (χ_{hf}) increase, whereas low-field susceptibility (χ_{lf}), natural remanent magnetization intensity and saturation magnetization (M_s) generally decrease with increasing oxidation state.

Key words: hysteresis parameters, maghemitization, NRM intensity, oceanic basalts.

1 INTRODUCTION

The magnetization of the oceanic crust has remained of fundamental importance to the theories of seafloor spreading and plate tectonics ever since Vine & Matthews (Vine & Matthews 1963) first demonstrated that the magnetic anomalies paralleling the mid-ocean ridges could convincingly be interpreted as a record of the geomagnetic polarity timescale. And yet, the magnetic carriers in the pillow

basalts of the oceanic crust demonstrably undergo widespread oxidation to titanomaghemite, presenting the paradoxical situation that apparently the original magnetic record stays well preserved while the carriers of this record undergo such fundamental mineralogical transformations that one would expect secondary magnetizations and chaotic anomaly patterns to be the rule rather than the exception. As a solution to this paradoxical dilemma, it has been suggested (see discussions in Beske-Diehl 1990; Dunlop & Özdemir

1997: pp. 399–400) that during oxidation of titanomagnetite to titanomaghemite, the magnetic directions of the new minerals mimic the previous directions, but this has not been confirmed by convincing experimental work on natural samples.

During oxidation, moreover, it appears that the magnetic intensity of the natural remanent magnetization (NRM) in mid-oceanic ridge basalt (MORB) generally diminishes. Variations in the amplitudes of magnetic anomalies have been attributed to large-scale variations in NRM intensities over the past 160 Ma (Bleil & Petersen 1983; Irving 1970; Johnson & Pariso 1993; Marshall & Cox 1972; Sayanagi & Tamaki 1992). Thus, it is logical that, in turn, the decrease in anomaly amplitude with increasing age has been attributed to increasing oxidation of the Fe–Ti oxides (see Dunlop 1995), but this inference remains highly controversial. Other factors, such as viscous decay of the remanence (Banerjee 1971), geomagnetic field intensity fluctuations (Gee & Kent 1998), or basaltic composition with variable Fe content (Gee & Kent 1997; Vogt & Johnson 1973) cannot be easily discounted.

In order to make progress in resolving questions about magnetic intensities and the stability of magnetic directions, despite prevalent oxidation to non-stoichiometric Fe–Ti oxides, further studies of the effects of maghemitization are necessary. But here one quickly encounters problems resulting from the fact that many parameters change in parallel fashion, but for very different reasons, and that cause and effect attributions can, therefore, not be considered unique. As an example, we cite the well-known variation in Curie temperature (T_c), which increases with decreasing Ti content (decreasing x) in titanomagnetite, but also with increasing oxidation (increasing z) to titanomaghemite (Nishitani & Kono 1983). Without sophisticated transmission electron microscopy (TEM) (e.g. Zhou *et al.* 1999a) it is possible to estimate oxidation state (i.e. z) only for relatively large grains that do not necessarily carry stable remanence.

A promising approach was taken by Beske-Diehl & Soroka (1984) and Beske-Diehl (1990), who used large variably altered pillow fragments, so that the effects of varying grain size, ancient geomagnetic

field intensity, and initial composition could be assumed to have not played a role in variations in various rock magnetic parameters. However, they had to assume (for lack of analytical tools to determine otherwise) that the alteration rims uniformly contained more highly oxidized Fe–Ti oxides than the apparently unaltered pillow interiors. In this study, we follow the sampling approach of Beske-Diehl, but use electron-microscopic determinations of composition x and lattice parameters to determine z for individual grains of sizes as small as 0.3 μm.

2 SAMPLES AND ANALYTICAL TECHNIQUES

A suite of MORB samples from the East Pacific Rise (EPR) was dredged during the Phoenix expedition (Batiza *et al.* 1996), and nine of these samples, varying in age from ~200 ka to ~820 ka, were selected for this study. The samples were kindly provided by colleagues or obtained from the collections at the Scripps Institute of Oceanography (SIO) of the University of California, San Diego. Table 1 lists localities, ages, T_c, composition x and oxidation state z, the latter as estimated from x-values and lattice parameters. Ages of the samples were estimated from their distance to ridge axes, given the known spreading rates. It is estimated that there may be error margins of about 40 000 yr on these ages, given that the volume of material erupted more than 2 km from the axis is likely to be negligible (Batiza *et al.* 1996). The sample labels (e.g. in our tables and figure captions) follow the original SIO scheme. Additional letters (a–j) after the numbers of the samples indicate subsample position within a pillow fragment, where each letter represents a distance from the outer glassy pillow margin at increments of ~1 cm. The letters in parentheses (f = fresh, or w = weathered), indicate whether the subsample came from the relatively unaltered grey interior or from the discoloured rim. Finally, the last two sets of numbers (1–14 and I–VIII) are used for subsamples ph19g and ph19e and indicate data collected in traverses from one crack boundary to the other, parallel to the pillow's glassy margin, as will be detailed below.

Table 1. Oxidation state of paired M ORB subsamples.

Age[†], ka	Sample	Latitude	Longitude	T_c, °C	x_{AEM}	Std, x_{AEM}	n_{AEM}	x_{probe}	Std, x_{probe}	n_{probe}	a, Å	z
Subsamples from grey interiors												
206	ph114e (f)	11.3	−103.90	132	0.68	0.03	18	0.624	0.04	4	8.474	0.26
382	ph88e (f)	11.4	−103.60	176	0.71	0.02	7	0.689	0.04	9	8.460	0.47
437	ph119e (f)	11.3	−103.97	227	0.69	—	—	0.646	—	—	8.455	0.54
510	ph78e (f)	10.4	−103.90	135	0.72	0.03	10	0.690	0.05	6	8.463	0.47
568	ph122e (f)	11.3	−104.03	225	0.68	—	—	0.600	—	—	8.460	0.38
578	ph39e (f)	9.50	−104.50	310	0.59	0.06	17	0.584	0.05	7	8.453	0.40
747	ph123f (f)	11.3	−104.11	207	0.64	—	—	—	—	—	8.462	0.25
800	ph19g (f)	9.50	−103.90	230	0.76	0.04	11	0.731	0.03	5	8.436	0.73
823	ph124f (f)	11.3	−104.15	296	0.65	—	—	0.621	—	—	8.441	0.55
Subsamples from discoloured rim s												
206	ph114e (w)	11.3	−103.90	210	0.69	0.05	17	0.664	0.03	13	8.445	0.69
382	ph88e (w)	11.4	−103.60	241	0.72	0.04	12	0.692	0.02	6	8.433	0.71
437	ph119e (w)	11.3	−103.97	255	0.68	—	—	0.584	—	—	8.427	0.66
510	ph78e- f (w)	10.4	−103.90	195	0.71	0.04	11	0.690	0.02	7	8.429	0.75
568	ph122e (w)	11.3	−104.03	256	0.67	—	—	0.639	—	—	–	
578	ph39e (w)	9.50	−104.50	313	0.60	0.04	18	0.534	0.05	10	8.432	0.57
747	ph123f (w)	11.3	−104.11	273	0.64	—	—	—	—	—	8.457	0.48
800	ph19g (w)	9.50	−103.90	267	0.77	0.04	15	0.767	0.03	5	8.436	0.75*
823	ph124f (w)	11.3	−104.15	290	0.66	—	—	0.586	—	—	8.426	0.54

[†]: Age was estimated from the distance to the spreading centre. The Brunhes/Matuyama is set to be 0.78 Ma.

*: The z-value for sample ph19 is listed only for the more interior subsamples from the discoloured rim (see text for discussion).

[‡]: Paired subsamples are denoted by (f) and (w) for the grey interior and the discoloured rim, respectively.

Variables: x_{AEM}, x-value from AEM analyses; Std, x_{AEM}, standard deviation of x-value from AEM analyses; x_{probe}, average x-value from electron microprobe.

Rock magnetic and palaeomagnetic parameters, such as saturation remanence (M_{rs}), saturation magnetization (M_s), coercive force (H_c), coercivity of remanence (H_{cr}), low-field susceptibility (χ_{lf}) and NRM intensity (J_{NRM}), all strongly depend on grain size, domain state, composition and mineralogy of the magnetic carriers. Grain size and composition can vary systematically as a function of depth from the glassy outer margin of a pillow (Gee & Kent 1997; Marshall & Cox 1971; Zhou *et al.* 2000). By taking subsamples parallel to the glassy margin within a pillow, it becomes possible, however, to evaluate directly the role of low-temperature alteration on the changes of magnetic properties with minimum interference from systematic variations in grain size and composition. When we began our study, we anticipated that the maximum difference in low-temperature alteration would occur between the outermost part of the discoloured rim and the middle of the grey interior, and the paired samples that we analysed initially were located accordingly within the nine studied pillows (e.g. Fig. 1).

Polished thin sections were prepared for optical and scanning electron microscopy (SEM). SEM observations were made with a Hitachi model S3200N fitted with secondary electron and backscattered electron (BSE) imaging systems. Ion-milled samples, obtained from the thin sections, were used for TEM and analytical electron microscopy (AEM), carried out with a Philips CM-12 TEM fitted with
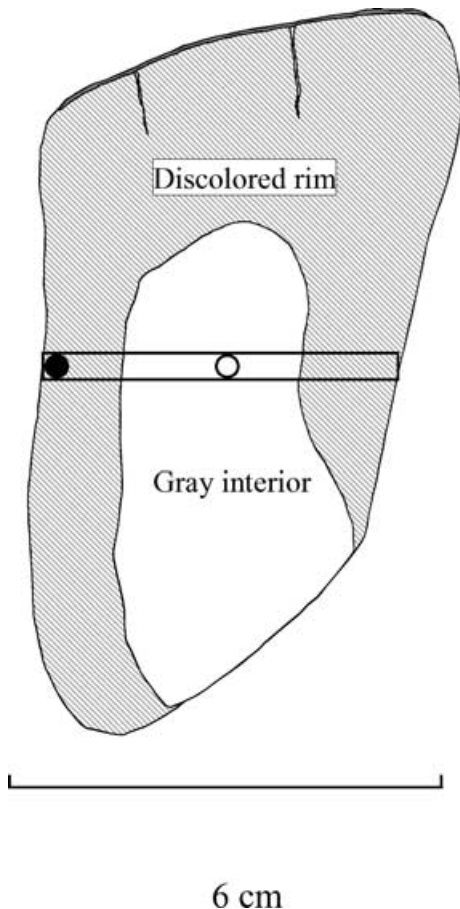
Figure 1. A typical cross-section of a variably altered fragment of pillow basalt, sample ph124, ∼820 000 yr old. An alteration halo has formed around three sides of the fragment, with the left- and right-hand side representing boundaries due to cracks that penetrated into the pillow. We investigate whether the oxidation degree of Fe–Ti oxides in the discoloured rim (closed symbols) is higher than in the grey interior (open circles), by analysing subsamples for TEM and rock magnetic analysis.

a Kevex Quantum EDS system and operated at 120 KV. The values of *x* were calculated from AEM analyses (see Zhou *et al.* 1999a, for details). The degree of oxidation of a single titanomaghemite grain (*z*) is determined from its lattice parameter (*a*) and composition (*x*) (Nishitani & Kono 1983; Readman & O'Reilly 1972; Zhou *et al.* 1999a). A TEM technique in convergent-beam electron diffraction mode (CBED), called higher-order Laue zone (HOLZ) lines, was employed to accurately measure lattice parameters of individual titanomagnetite grains (Zhou *et al.* 1999a). For grains larger than 5 μm in sample ph78, a Cameca electron microprobe model SX100 was used, because with this instrument oxygen can be included in the elemental analysis, and this, therefore, allows us to estimate *z*, as described by Furuta (1993) and Zhou *et al.* (1999a).

To verify values of the Ti content (*x*), in addition to its determination by the AEM analyses, several other samples were also analysed with a Cameca electron microprobe, model SX100. The *x*-values obtained by the two techniques are compared in Table 1.

NRM of bulk-rock samples was measured using a 2G cryogenic magnetometer at the University of Michigan. Low-field susceptibility was measured using a Geofyzika Kappabridge, model KLY-2, calibrated by an etalon standard. AF demagnetization of NRM was performed using a Sapphire Instruments SI-4 AF demagnetizer. Rock magnetic parameters were measured at the Institute for Rock Magnetism (IRM) at the University of Minnesota. Hysteresis parameters of bulk-rock samples were measured on a vibrating sample magnetometer (VSM). Curie temperatures (*Tc*) were determined from a linear extrapolation of high-field (800 mT) thermomagnetic curves (Grommé *et al.* 1969) using a VSM. The thermomagnetic curves were measured on a small rock chip of about 40 mg while heating in noble gas.

3 RESULTS

3.1 Petrology; electron-microscope observations; determinations of *x* and *z*

Different features of alteration rims have been described (Alt 2004; Alt & Teagle 2003), and include alteration phases in the following order of appearance:

(1) celadonite fill of void spaces in a dark alteration halo,

(2) Fe-oxyhydroxide staining under oxidizing conditions in the rims that become lighter-coloured than the interiors, while the latter retain a reducing environment and

(3) saponite (a Mg-rich and Fe^{2+}-containing variety of the smectite family of clay minerals) and pyrite formation in fractures and the formation of carbonate veins throughout the rock. The discoloured rims in our samples are characterized by extensive precipitation of secondary minerals as vesicle fillings (Fig. 2b) and the halos are darker than the interiors, indicating that we are dealing with alteration phase (1), as described above. In a few samples, hints of lighter discolouration are observed, but Fe-oxyhydroxide staining is not readily observable. The main secondary mineral is the Fe^{3+}-rich clay mineral celadonite, containing minor amounts of K, Al and Mg. The clays usually show mottled features and appear in the SEM images surrounded by a thin gap due to dehydration in the instrument's vacuum. Near the side edges of the pillow fragments (i.e. near the cracks), energy-dispersive spectra (EDS) of the clay domains sometimes give rise to relatively high Fe and O peaks in EDS analyses, possibly indicating minor amounts of Fe oxyhydroxides, whereas towards the interior no evidence for Fe oxyhydroxides is seen.
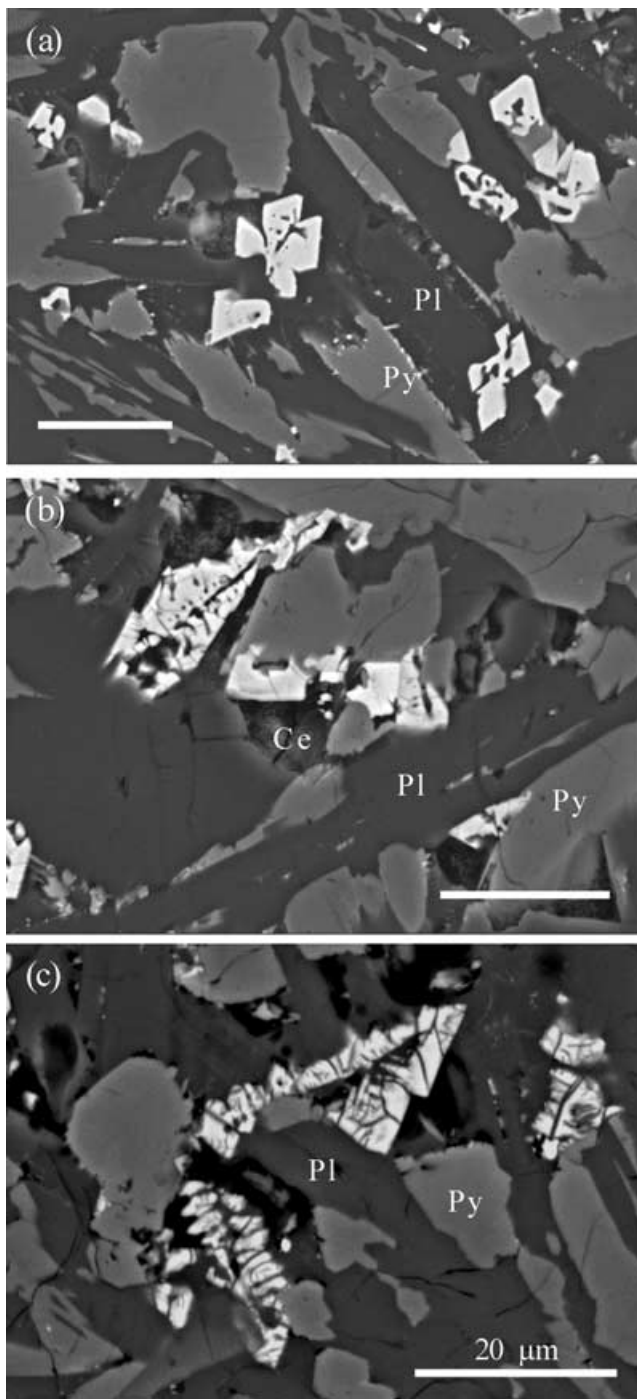
Figure 2. SEM back-scattered electron images of basalt pillow ph19 ($\sim$800 ka). Pl = plagioclase, Py = pyroxene. (a) Ti–Fe-oxide grains in the outermost part of the discoloured rim, showing few signs of oxidation, which is confirmed by our determination of a relatively low degree of oxidation (z = 0.36). (b) Highly oxidized titanomaghemite grains from the discoloured rim. Void spaces have typically been filled by secondary clay minerals (e.g. Ce = celadonite). (c) Highly oxidized titanomaghemites from the grey interior, surrounded in part by still-open void spaces (darkest areas).

SEM backscattered electron images of selected subsample pairs show that the average sizes of titanomagnetite grains are approximately the same in grey interiors and in discoloured rims (Fig. 2). Considerable oxidation of titanomagnetite is observed

in the alteration rim as well as in the grey interior of this $\sim$800 ka old sample (Table 1). Because lattice parameters generally decrease with increasing degree of oxidation (Nishitani & Kono 1983; Readman & O'Reilly 1972), shrinkage cracks have been commonly observed in natural samples as a result of heterogeneous oxidation (e.g. Johnson & Hall 1978; Petersen & Vali 1987). The smaller, diffuse cracks interior to the oxide grains in Fig. 2(c) may also be taken as an indication of oxidation. Judging from the observed maghemitization (to be discussed further below), oxidation of the Fe–Ti oxides proceeded throughout the sample regardless of the presence or absence of oxidizing conditions inferred from the clays.

AEM analyses yielded x values (averages listed in Table 1) for titanomaghemite grains in discoloured rims and grey interiors from nine subsample pairs (configured as in Fig. 1). Differences in x between the nine different pillow fragments are significant and no apparent trend is observed for x as a function of sample age (Table 1). In order to obtain independent estimates of x, we utilized an electron microprobe to analyse relatively large grains. The values so obtained are also listed in Table 1; the x_{probe} values are systematically lower by about 6 per cent on average compared to the x_{AEM} values. We do not know the reason for this difference, but speculate that oxidation of the smaller grains may be slightly greater than that of the larger grains analysed with the electron microprobe; given that maghemitization reduces the Fe/Ti ratio and hence increases x, the AEM results may be greater because the grain sizes analysed with this technique may have been, on average, somewhat smaller.

The oxidation state (z) of titanomaghemite grains can be determined from their lattice parameter (a) and composition (x), as described by Zhou *et al.* (1999a). HOLZ line patterns obtained in CBED mode with the TEM (Zhou *et al.* 1999a) were used to determine lattice parameters for representative grains. We used these values for a and the x_{AEM} values for the calculation of z. The averaged z-values for the subsample pairs so obtained are listed in Table 1; z-values plotted in Fig. 3(a) include analyses of several grains per sample and have not been averaged. The values of T_c are also plotted in Fig. 3 as a function of sample age. Of course, these Curie temperatures were obtained on finite-sized samples and, therefore, they represent the 'average' of large numbers of Fe–Ti-oxide grains.

With increasing sample age, the differences in z between grains from the discoloured rim and grey interior becomes smaller: the youngest sample ($\sim$206 ka, sample ph114) shows a much larger difference in z than the older samples (Fig. 3a). The difference in oxidation states between rim and interior becomes negligible for samples ph19 and ph124 ($\geq \sim$800 ka).

The differences in x-values between rim and core can be seen in the ternary diagrams of Fig. 4, which illustrates that the increased oxidation of rim samples has led to slightly elevated x-values in some samples; nevertheless, we grant that there is sufficient scatter in the results of Fig. 4(b) and (c) to argue that this effect is not always significant. The same conclusions about oxidation state can be reached by examining the Curie temperatures for pairs of subsamples in Fig. 3(b). We also note that Curie temperatures show an increasing trend with increasing age, as consistent with results from previous studies (Bleil & Petersen 1983; Irving 1970; Xu *et al.* 1997), although z and Tc values vary significantly from sample to sample. There is considerable scatter in the diagrams of Figs 3 and 4, because of variations in x and z from grain to grain, whereas Curie temperature measurements are made on sample chips that average the properties of many grains.
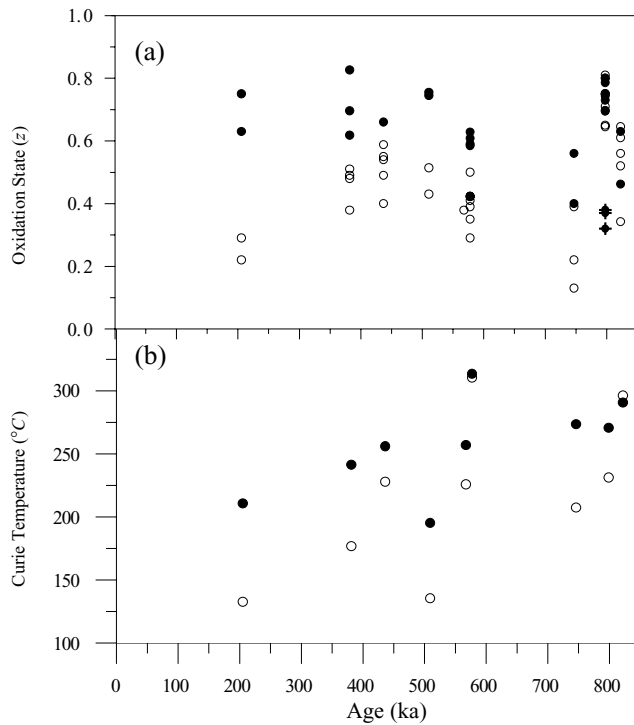
Figure 3. Oxidation state of individual grains and Curie temperatures of subsamples from nine pillow fragments, plotted versus age. Dots represent data from discoloured rims, open circles from grey interiors. (a) Oxidation degree (z) obtained by TEM and AEM study of titanomaghemite grains. Dots with a + represent anomalously low z values from a 1-mm-thick dark outermost zone of the discoloured rim of sample ph19 ($\sim$800 ka). (b) Curie temperatures of subsamples.

3.2 Thermomagnetic results

The saturation magnetization (M_s) measured in a field of 800 mT as a function of temperature for all but two of our samples showed irre-

versible thermomagnetic curves that are typical of titanomaghemite (Fig. 5). The two exceptions were for samples ph114(f) and ph123(f), where the reversible nature of the thermomagnetic curves is in good agreement with the behaviour of samples with z-values less than 0.30 (see Table 1 and Fig. 3a) as described in the literature (Grommé *et al.* 1979).

For all the other subsamples ($z > 0.35$), heating curves are generally similar, either in grey interiors or in discoloured rims, and show T_c values generally greater than 200°C, followed by an increase of M_s in the heating curves above 380°C. This behaviour is usually attributed to new growth of Fe oxide during treatment (Özdemir 1987; Ozima 1971). The thermomagnetic curve of a sample with one of our higher oxidation parameters ($z = 0.75$) is illustrated in Fig. 5b and shows a convex upward cooling curve characteristic of abundant new-formed low-Ti magnetite. In general, all the samples from the discoloured rims show this behaviour during cooling from 650°C.

## 3.3 Variations in rock magnetic properties

Some hysteresis parameters and susceptibility values are plotted in Fig. 6 as a function of oxidation state for seven pairs of subsamples from discoloured rims (full dots) and grey interiors (open symbols). The data are listed in Table 2; note that one pair (sample ph19, $\sim$800 ka) is discussed separately and in great detail below, and that the ninth pair (sample ph122e) lacks a z-value (see Table 1). Sample ph19 is discussed separately because of its unusually large variation in z in the discoloured rim (see Fig. 3a at 800 ka) and its unusually high average x-values of 0.73–0.77 (Table 1), which makes this sample a clear anomaly.

The plots of Fig. 6 show generalized trends for four parameters (M_s, H_c, χ_{lf}, and χ_{hf}). H_{cr} (not plotted, but listed in Table 2) tracks H_c (Fig. 6c) and shows a very similar trend of increasing values with increasing z.

Increases in bulk coercivity (H_c) and coercivity of remanence (H_{cr}) with increasing oxidation state have been reported before
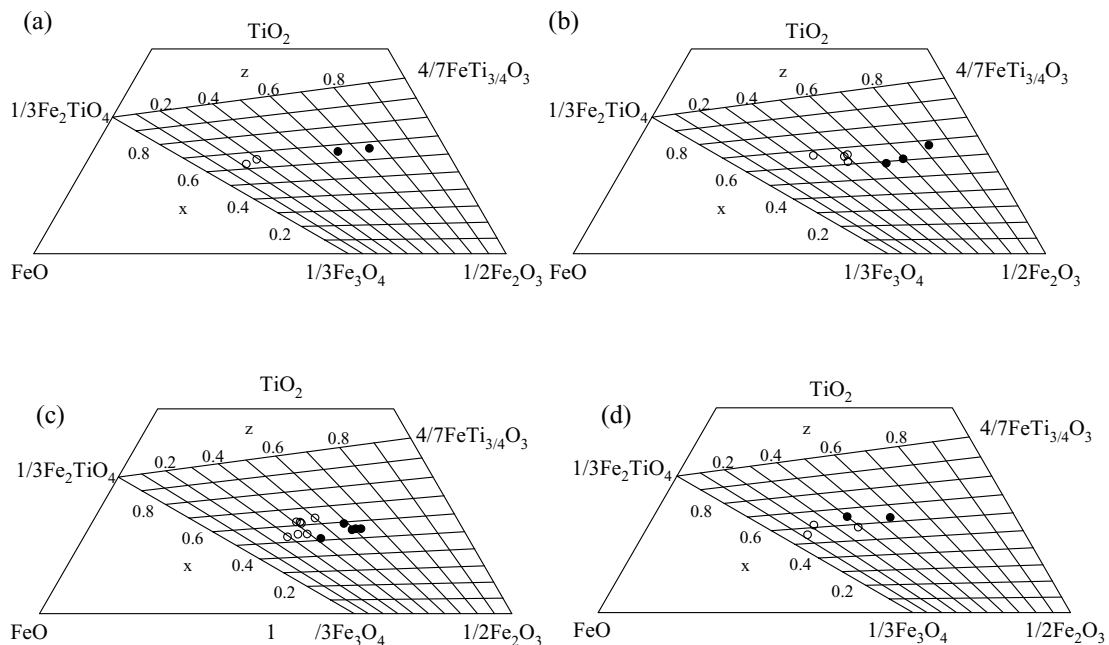
Figure 4. Projection of measured x values and estimated z values for individual grains on TiO$_2$-FeO-γFe$_2$O$_3$ ternary diagrams, showing the difference between grains in the discoloured rim (closed symbols) and those in the grey interior (open symbols). (a) Measurements for sample ph114. (b) Sample ph88. (c) Sample ph39. (d) Sample ph123.
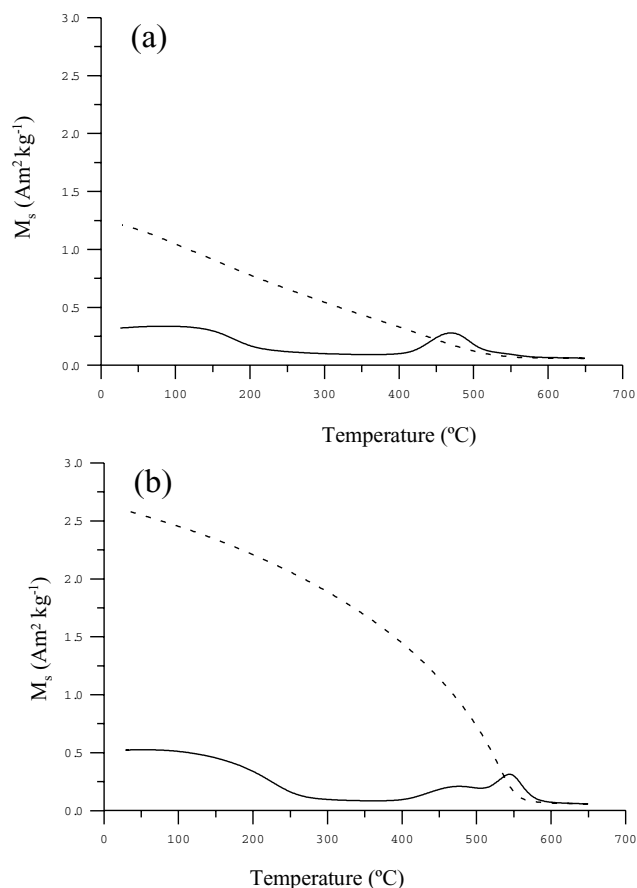
Figure 5. Representative thermomagnetic curves from subsamples of variably altered pillow fragment ph19 (∼800 ka). The magnetic saturation is measured by a vibrating sample magnetometer using a field of 800 mT. (a) grey interior and (b) discoloured rim. Solid lines represent heating, dashed lines cooling curves.

(Dunlop & Özdemir 1997). Beske-Diehl (1990) shows such increases for samples with $Tc < 320°C$, which is the case for all our samples (Table 1). The increase in H_c in natural samples has been attributed to fracturing induced domain-size reduction (Dunlop & Özdemir 1997: pp. 401–402) or to magnetostriction caused by volume changes during maghemitization of natural samples with $x \approx 0.55$ and $z \approx 0.9$ (Hodych & Matzka 2004). On the other hand, H_c is known to decrease in synthetic samples for $z > 0.55$ (Dunlop & Özdemir 1997: Fig. 3.19).

Lower M_s intensities are generally expected for oceanic basalts with higher degrees of oxidation (Dunlop & Özdemir 1997: Fig. 3.18), and our observations confirm this. Lower M_{rs} intensities are less frequently discussed, but the values of M_{rs} that can be calculated from the parameters in Table 2 of Beske-Diehl show decreases in more than 80 per cent of her sample pairs (Beske-Diehl 1990). In our samples decreases of M_{rs} with increasing z (not shown) are not convincing.

The low-field susceptibility (χ_{lf}) generally decreases with oxidation state (Fig. 6b), in agreement with previous observations (Beske-Diehl 1990; Johnson & Hall 1978). High-field susceptibility (χ_{hf}), also known as the paramagnetic correction applied to hysteresis curves, represents the paramagnetic content in the rock and increases with increasing z (Fig. 6d).

Thus far, our discussion of the correlations between oxidation state and rock magnetic parameters has proceeded for the seven subsample pairs that show behaviour according to expectations of higher oxidation of the rims (Fig. 6). However, one of our oldest samples (ph19, ∼800 Ka) behaved anomalously and discussion of its properties was, therefore, deferred. We now discuss the nature of this sample, which—importantly—made us realize that a correlation between pillow-rim discolouration and the oxidation state of the Fe–Ti oxides exists only in a most general way but not in detail.

3.4 A detailed traverse through anomalous sample ph19

Because of unusually large variations in z in its discoloured rim (Fig. 3a), sample ph19 (∼800 ka) became the subject of a special study in which we determined rock magnetic parameters and x-values in a much more detailed traverse as illustrated in Fig. 7(a). A second, partial traverse (Fig. 7b) was added later to determine z-values, and a different sample (ph78) was examined in a similar partial traverse to ensure that the behaviour of sample ph19 was indeed anomalous. Data for sample ph19 are reported in Tables 3 and 4 and illustrated in Fig. 8. The results from the first traverse of the pillow fragment of ph19 (Fig. 7a, subsamples ph19g(f&w), 1–14) displayed large variations in all hysteresis parameters as well as NRM intensity. It turns out that the anomalous values correlate with anomalously low z-values of about 0.36 in three grains at the outer edge of the discoloured rim (Fig. 7b, subsample ph19e(w)-I; Table 4), compared to z-values from all other subsamples either in the discoloured rim or in the grey interior (Fig. 8, bottom diagram), which range from 0.70 to 0.81 without any systematic trend.

The data of Fig. 8 provide a clear indication that z does not at all correlate with the alteration in the discoloured rims because no pronounced changes are observed at the discolouration front next to the grey interior. The z values of titanomaghemite grains in discoloured rim subsamples close to the alteration front are not significantly different from those of the adjacent subsamples inside the grey interior.

Fig. 8 also reveals that at the other side of the pillow a more or less symmetrical situation is observed, which even includes an outermost subsample with relatively higher M_s, M_{rs}, NRM and χ_{lf} values, and lower H_c and H_{cr} values, indicating that our observations of subsamples ph19g(f)-8 to ph19g(w)-14 are mirrored on both sides of the pillow fragment. We have, by the way, no satisfactory explanation for the low oxidation state of the three grains at the outermost edge of the pillow.

3.5 Variations in NRM intensities

One further observation is noteworthy, and that is that the measurements of the NRM intensity at the millimetre scale of these traverses (Fig. 8 top) reveal a good (inverse) correlation between z and NRM intensity. Our initial NRM measurements on the rims of the nine pillow fragments (as listed in Table 2) used larger subsamples, several centimetres in size, resulting in gross averaging of the contributions from grains with possibly a wide range of z-values. To test the more detailed variations and to augment the dataset, we also measured J_{NRM} and z (with the microprobe) of sample ph78. The values from these two millimetre scale traverses are plotted in Fig. 9. Although it must be noted that the clear correlation between a high degree of oxidation and a lower NRM intensity should be seen as qualitative only, because the measurements of NRM are for finite-sized subsamples (whereas z is determined on a small set of grains), this nevertheless clearly illustrates that increased oxidation of the Fe–Ti oxides results in diminished NRM intensities. This is not a new conclusion, because Beske-Diehl (1990) had already reported that
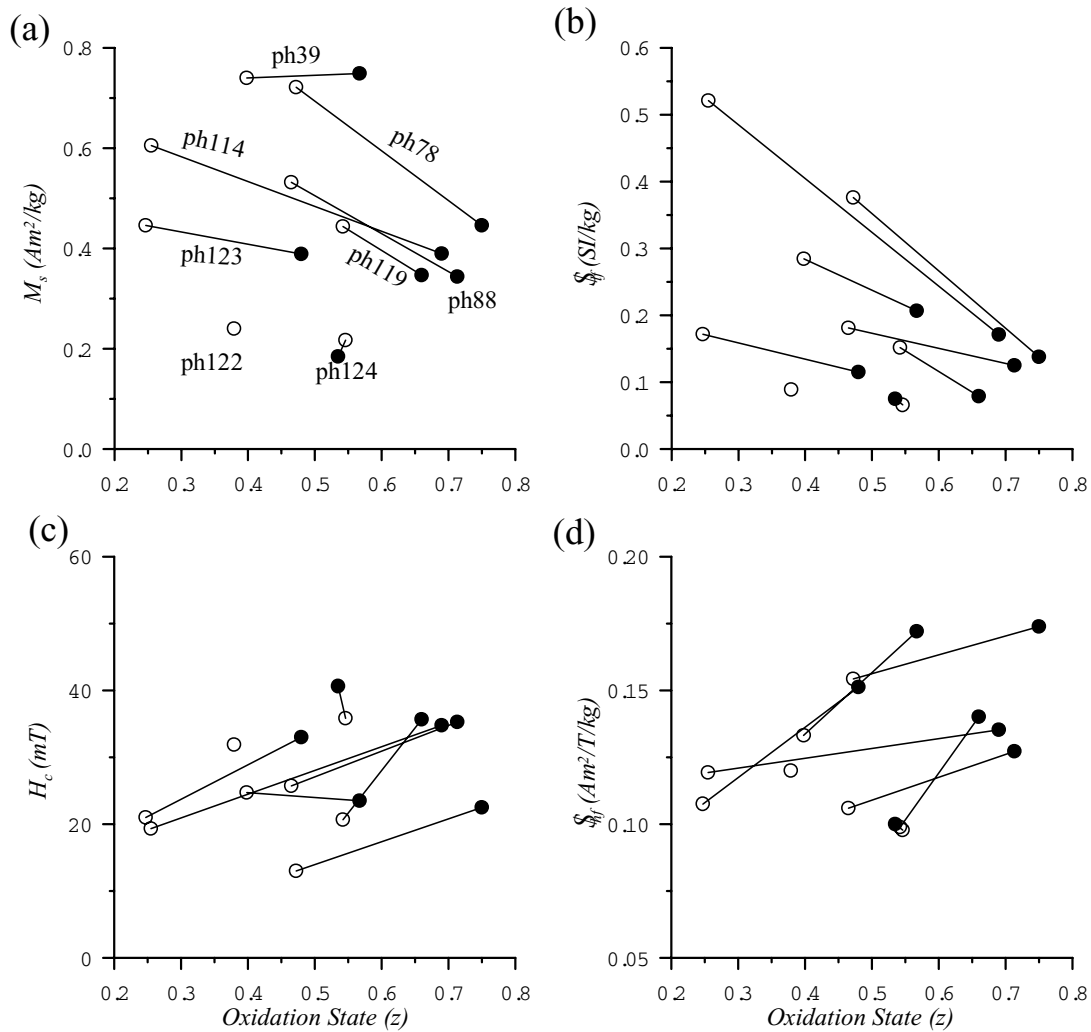
Figure 6. (a) Saturation magnetization (M_s), (b) low-field susceptibility, (c) coercive force and (d) high-field susceptibility (i.e. paramagnetic correction) all plotted as a function of oxidation degree (z). Open circles represent subsamples from grey interiors and filled symbols represent subsamples from discoloured rims. Subsamples from the same pillow fragment are connected by a straight line; note that one pillow fragment (ph122, ~570 ka) lacks a z-value for its rim. Anomalous sample ph19 is not included in these plots, as its properties are better displayed in a separate figure (Fig. 8). Values are listed in Tables 1 and 2.

all her samples showed decreases in NRM intensity with increasing T_c (used as a proxy for z).

4 DISCUSSION AND CONCLUSIONS

4.1 Characterizing the oxidation state of Fe–Ti oxides in MORB

We have learned from the present study that alteration of pillow rims, seen as discoloured halos, does not predict with any accuracy what the oxidation state of the Fe–Ti oxides may be. Even though, in general, darker discoloured rims contain more highly oxidized titanomaghemite, any correlation between z and visible alteration due to celadonite filling void spaces is coincidental, as the results in Fig. 8 demonstrate. A greater degree of rim alteration (phases 2 and 3 of Alt & Teagle 2003) may correlate better with oxidation, as suggested by the data of Böhlke and colleagues (Böhlke et al. 1981), who studied MORB formed ~10 Ma in the Atlantic Ocean. In some of their samples oxidation has even proceeded to cause breakdown of titanomaghemite to non-magnetic oxides.

Because Curie temperature variations may also reflect changes in x, their use as proxies for oxidation state may give imprecise results. Instead, direct determinations of the z-values of titanomaghemite are desirable in order to investigate the effects of oxidation on rock magnetic parameters. This can be achieved with an electron microprobe but only on relatively large grains ($> 5 \mu$m) (Akimoto et al. 1984; Furuta 1993; Zhou et al. 1999a). More suitable techniques employed by us in recent years allow calculations of the z-value on the basis of its relationship with a and x, but this requires accurate calibration of the relationship (see Zhou et al. 1999a, and references therein). The diameter of the electron beam limits the determination of a to grains of a certain minimum size, which is typically $> 1 \mu$m for conventional selected-area electron diffraction (SAED); in contrast, HOLZ line patterns can be obtained on grains potentially as small as 0.1 μm, although even this may not be small enough in some cases. Powder X-ray diffraction through Rietveld refinement (Xu et al. 1997) is another technique to determine a, but does not allow re-use of the same sample for later, different measurements. In addition to these methods, a recent innovative proposal involves quantification of ferrous/ferric ratios using electron energy

Table 2. Rock magnetic properties of paired subsamples.

Sample	H_c, mT	H_{cr}, mT	M_s, A m^2 kg^{-1}	M_{rs}, A m^2 kg^{-1}	H_{cr}/H_c	M_{rs}/M_s	NRM, 10^{-3} A m^2 kg^{-1}	χ_{lf}, SI/kg	χ_{hf}, A m^2/T/kg[†]
ph114e (f)	19	26	0.61	0.22	1.35	0.36	1.37	0.521	0.12
ph88e (f)	26	33	0.53	0.23	1.29	0.42	1.92	0.181	0.11
ph119e (f)	21	28	0.44	0.16	1.36	0.36	3.40	0.152	0.10
ph78e (f)	13	22	0.72	0.21	1.67	0.29	1.19	0.376	0.15
ph122e (f)	32	42	0.24	0.11	1.32	0.47	2.55	0.089	0.12
ph39e (f)	25	37	0.74	0.18	1.50	0.25	1.22	0.284	0.13
ph123f (f)	21	27	0.45	0.18	1.29	0.40	6.00	0.172	0.11
ph19g (f)	56	70	0.17	0.10	1.23	0.57	0.40	0.054	0.13
ph124f (f)	36	42	0.22	0.10	1.17	0.47	0.12	0.066	0.10
ph114e (w)	35	44	0.39	0.18	1.28	0.45	0.94	0.171	0.14
ph88e (w)	35	47	0.34	0.16	1.32	0.46	2.13	0.125	0.13
ph119e (w)	36	44	0.35	0.17	1.23	0.49	3.86	0.079	0.14
ph78e (w)	22	33	0.45	0.18	1.49	0.40	0.85	0.138	0.17
ph122e (w)	32	40	0.28	0.13	1.24	0.47	0.98	0.037	0.13
ph39e (w)	24	32	0.75	0.21	1.34	0.29	3.47	0.207	0.17
ph123f (w)	33	41	0.39	0.18	1.25	0.45	5.89	0.115	0.15
ph19g (w)*	55	72	0.22	0.12	1.31	0.52	0.53	0.065	0.15
ph124f (w)	41	50	0.18	0.09	1.23	0.50	0.30	0.075	0.10

[†]: χ_{hf} is weight normalized high-field paramagnetic correction at a standard 70 per cent.

*Due to their abnormal oxidation states, subsamples ph19g-1 and ph19g14 are excluded from the average.
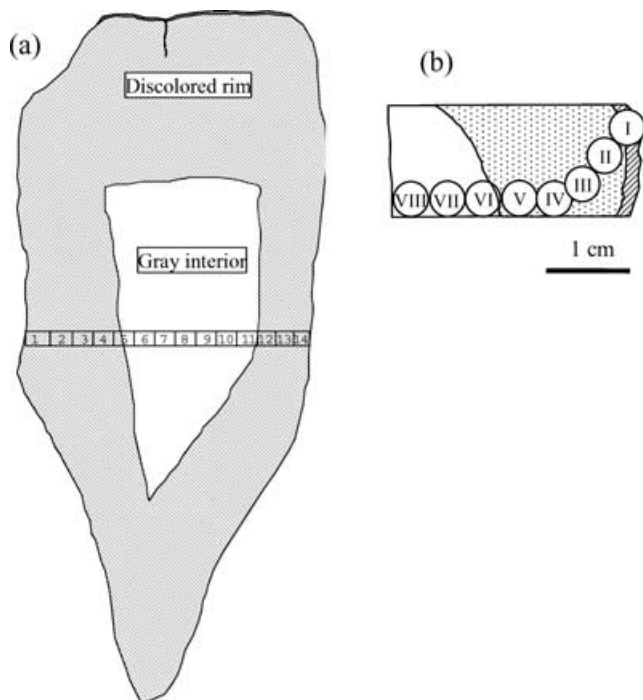
Figure 7. Sketch of subsample position for rock magnetic and electron microscopy measurements within pillow fragment ph19 ($\sim$800 ka). (a) A series of (14) subsamples along a traverse at 7 cm from the pillow's glassy margin. (b) Subsample positions for TEM study in a traverse at 5 cm from the glassy margin.

loss near-edge spectra. This may provide the oxidation state of titanomaghemite at high spatial resolution (van Aken & Liebscher 2002).

Low-temperature oxidation of MORB has now been investigated for more than three decades for natural samples (e.g. Böhlke *et al.* 1981; Irving 1970; Kent & Gee 1994; Zhou *et al.* 2001) and synthetic samples (Brown 1981; Kelso *et al.* 1991; Özdemir & Dunlop 1985; Worm & Banerjee 1984), and much debate has centred on

the rate at which oxidation proceeds, with estimates for the time it takes to reach $z > 0.6$ ranging from 20 ka (Kent & Gee 1994) to some 500 ka (see discussion in Dunlop & Özdemir 1997: p. 398). It is likely that our own previous estimate of some 500 ka (Zhou *et al.* 2001) is too high and needs to be lowered to 200 ka or less (as can be seen from the z-value for our youngest rim sample in Fig. 3a).

It must be noted that some titanomagnetite grains of >30 Ma age are known to have escaped significant oxidation (Zhou *et al.* 1999b), so that the above estimates are clearly minima. It appears that the oxides could remain pristine in the Oligocene MORB, because of armouring by surrounding residual glass. In the present study, we have the puzzling finding of rather low z in the outermost rim of sample ph19(w). It is not at all clear to us how the oxides in this part of the pillow fragment could stay relatively unoxidized, while those in the interior became highly oxidized. Be that as it may, it once again shows that it is unwise to make assumptions about either x or z.

4.2 Changes of magnetic properties during low-temperature alteration

The observed trends and changes in rock magnetic properties as a function of increasing maghemitization are generally in good agreement with those of previous studies (e.g. Beske-Diehl 1990). Saturation magnetization (M_s), low-field susceptibility (χ_{lf}), and NRM intensity generally decrease, whereas bulk coercivity (H_c) and coercivity of remanence (H_{cr}) generally increase with increasing oxidation. In addition, paramagnetic correction values (high-field susceptibility (χ_{hf})) for discoloured rim subsamples were all higher than those of the corresponding grey interiors. The higher paramagnetic correction is consistent with the precipitation of paramagnetic Fe^{3+}-rich clay (celadonite) in the void spaces of the discoloured rims.

Initial NRM measurements were performed on larger basalt chips (several centimetres in size), whereas measurements of z where carried out on individual grains; this led to gross averaging and initially an apparent lack of correlation between increasing oxidation and decreasing J_{NRM}. However, when we measured subsamples on the

Table 3. Magnetic properties in a traverse in sample ph19 at a depth of 7 cm from the glassy rim.

Sample	H_c, mT	H_{cr}, mT	M_s, A m^2 kg^{-1}	M_{rs}, A m^2 kg^{-1}	H_{cr}/H_c	M_{rs}/M_s	NRM, 10^{-3} A m^2 kg^{-1}	χ_{lf}, SI/kg	TC, °C
ph19g-1	25.74	40.0	0.37	0.16	1.55	0.43	1.83	0.154	267
ph19g-2	52.10	68.9	0.21	0.11	1.32	0.52	0.44	0.065	236
ph19g-3	46.08	59.0	0.27	0.15	1.28	0.53	0.49	0.064	—
ph19g-4	49.82	64.0	0.18	0.10	1.28	0.55	0.41	0.050	243
ph19g-5	59.40	71.1	0.17	0.10	1.20	0.60	0.42	0.035	—
ph19g-6	55.54	63.7	0.11	0.08	1.15	0.73	0.39	—	227
ph19g-7	63.45	75.3	0.15	0.09	1.19	0.61	0.37	0.031	—
ph19g-8	56.28	69.5	0.15	0.09	1.23	0.57	0.39	0.044	230
ph19g-9	50.62	64.8	0.24	0.13	1.28	0.53	0.40	0.059	—
ph19g-10	49.87	63.9	0.20	0.11	1.28	0.54	0.40	0.062	—
ph19g-11	48.43	62.5	0.25	0.13	1.29	0.52	0.43	0.065	—
ph19g-12	55.33	72.6	0.21	0.11	1.31	0.52	0.44	0.067	—
ph19g-13	66.63	87.6	0.20	0.10	1.31	0.52	0.73	0.063	—
ph19g-14	19.98	29.0	0.58	0.24	1.45	0.42	2.53	0.229	—

Table 4. Oxidation state and chemical composition of titanomaghemites in subsamples of ph19 as shown in Fig. 7(b) and of three subsamples of ph78.

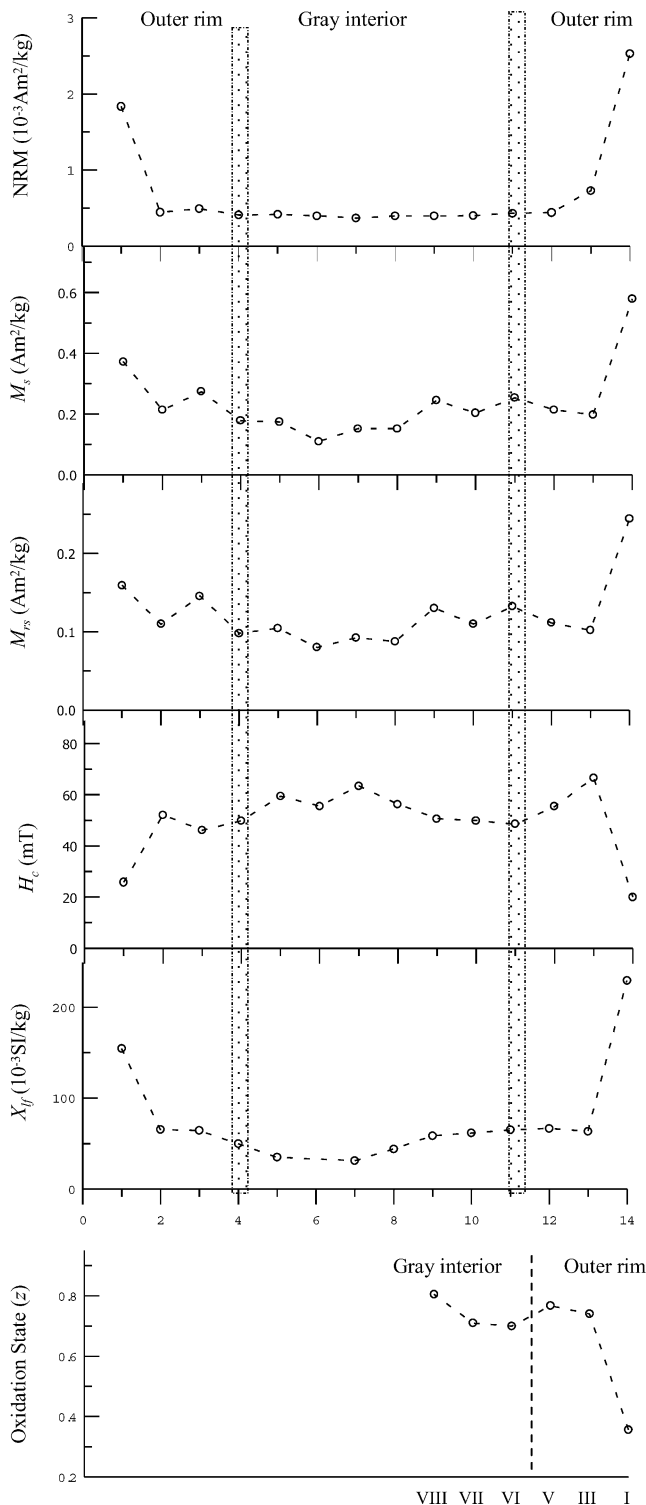| Properties	I	III	V	VI	VII	VIII	ph78-1	ph78-2	ph78-3
a	8.466	8.433	8.437	8.438	8.441	8.429	NA	NA	NA
x	0.68	0.73	0.77	0.73	0.74	0.76	0.75	0.70	0.67
x_{std}	0.01	0.02	0.02	0.01	NA	0.01	0.00	0.02	0.01
z	0.36	0.74	0.77	0.70	0.71	0.81	0.98	0.54	0.45
z_{std}	0.03	0.01	0.03	0.07	NA	0.01	0.05	0.06	0.11
n*	3	2	2	2	1	2	4	3	7

*: number of analyses.

millimetre scale, we find that NRM intensities of more highly oxidized subsamples are clearly lower than those of the less-oxidized samples (Fig. 9). This confirms the observations of previous studies that discoloured rims generally displayed a lower NRM intensity than grey interiors (Beske-Diehl 1990; Marshall & Cox 1972), but our study also illustrates that the discolouration front does not coincide with abrupt changes in oxidation.

REFERENCES

Akimoto, T., Kinoshita, H. & Furuta, T., 1984. Electron probe microanalysis study on processes of low-temperature oxidation of titanomagnetite, *Earth planet. Sci. Lett.,* **71,** 263–278.

Alt, J.C., 2004. Alteration of the upper oceanic crust: mineralogy, chemistry, and processes, in *Hydrogeology of the Oceanic Lithosphere,* pp. 456–488, eds Elderfield, H. & Davis, E., Cambridge University Press, New York.

Alt, J.C. & Teagle, D.A.H., 2003. Hydrothermal alteration of upper oceanic crust formed at a fast-spreading ridge: mineral, chemical, and isotopic evidence from ODP Site 801, *Chem. Geol.,* **201,** 191–211.

Banerjee, S.K., 1971. Decay of marine magnetic anomalies by ferrous ion diffusion, *Nature-Physical Science,* **229,** 181–183.

Batiza, R., Niu, Y., Karsten, J.L., Boger, W., Potts, E., Norby, L. & Butler, R., 1996. Steady and non-steady state magma chambers below the East Pacific Rise, *Geophys. Res. Lett.,* **23,** 221–224.

Beske-Diehl, S.J., 1990. Magnetization during low-temperature oxidation of seafloor basalts: no large scale chemical remagnetization, *J. geophys. Res.,* **95,** 21 413–21 432.

Beske-Diehl, S.J. & Soroka, W.L., 1984. Magnetic properties of variably oxidized pillow basalt, *Geophys. Res. Lett.,* **11,** 225–228.

Bleil, U. & Petersen, N., 1983. Variations in magnetization intensity of ocean floor basalts: reply, *Nature,* **306,** 92–92.

Böhlke, J.K., Honnorez, J., Honnorez-Guerstein, B.M., Muehlenbachs, K. & Petersen, N., 1981. Heterogeneous alteration of the upper oceanic crust: correlation of rock chemistry, magnetic properties, and O Isotope ratios with alteration patterns in basalts from site 396B, DSDP, *J. geophys. Res.,* **86,** 7935–7950.

Brown, K., 1981. Laboratory simulation of submarine maghemitization, *Geophys. J. R. astr. Soc.,* **65,** 273–273.

Dunlop, D.J., 1995. Magnetism in rocks, *J. geophys. Res.,* **100,** 2161–2174.

Dunlop, D.J. & Özdemir, Ö., 1997. *Rock magnetism: Fundamentals and Frontiers,* p. 573, Cambridge University Press, Cambridge, UK.

Furuta, T., 1993. Magnetic properties and ferromagnetic mineralogy of oceanic basalts, *Geophys. J. Int.,* **113,** 95–114.

Gee, J. & Kent, D.V., 1997. Magnetization of axial lavas from the southern East Pacific Rise (14°–23° S): geochemical controls on magnetic properties, *J. geophys. Res.,* **102,** 24 873–24 886.

Gee, J. & Kent, D.V., 1998. Magnetic telechemistry and magmatic segmentation on the southern east Pacific rise, *Earth planet. Sci. Lett.,* **164,** 379–385.

Grommé, S., Wright, T.L. & Peck, D.L., 1969. Magnetic properties and oxidation of iron-titanium oxide minerals in Alae and Makaopuhi lava lakes, Hawaii, *J. geophys. Res.,* **74,** 5277–5294.

Figure 8. Changes in magnetic properties in a detailed traverse across ph19 (∼800 ka), plotted versus subsample positions (as in Fig. 7a), as well as degree of oxidation (z) along the traverse of Fig. 7(b). Values are listed in Tables 3 and 4.
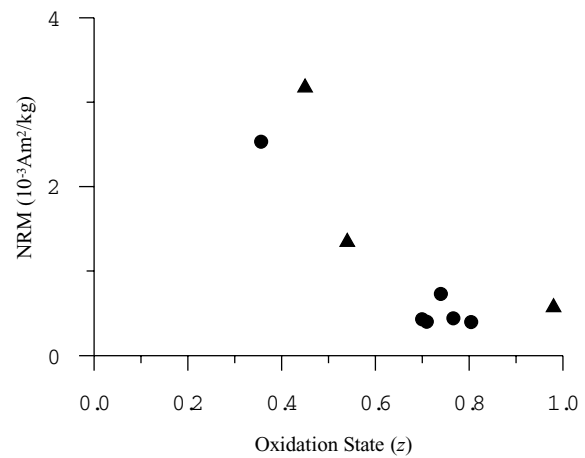
Figure 9. NRM intensity versus degree of oxidation (z). Circles represent subsamples from sample ph19, triangles from sample ph78; the three points for ph78 have the following z-values and NRM intensities (J_{NRM} in 10^{-3} A m^2 kg^{-1}): $z_1 = 0.98$ and $J_{NRM-1} = 0.6$; $z_2 = 0.54$ and $J_{NRM-2} = 1.37$; $z_3 = 0.45$ and $J_{NRM-3} = 3.2$.

temperature variation inferred for natural titanomaghemites: implications for internal stress control of coercivity in oceanic basalts, *Geophys. J. Int.,* **157,** 1017–1026.

Irving, E., 1970. The Mid-Atlantic Ridge at 45°N, XIV, oxidation and magnetic properties of basalts: review and discussion, *Can. J. Earth Sci.,* **7,** 1528–1538.

Johnson, H.P. & Hall, J.M., 1978. Detailed rock magnetic and opaque mineralogy study of basalts from Nazca Plate, *Geophys. J. R. astr. Soc.,* **52,** 45–64.

Johnson, H.P. & Pariso, J.E., 1993. Variations in oceanic crustal magnetization: systematic changes in the last 160 million years, *J. geophys. Res.,* **98,** 435–445.

Kelso, P.R., Banerjee, S.K. & Worm, H.U., 1991. The effect of low-temperature hydrothermal alteration on the remanent magnetization of synthetic titanomagnetites: a case for acquisition of chemical remanent magnetization, *J. geophys. Res.,* **96,** 19 545–19 553.

Kent, D.V. & Gee, J., 1994. Grain size-dependent alteration and the magnetization of oceanic basalts, *Science,* **265,** 1561–1563.

Marshall, M. & Cox, A., 1971. Magnetism of pillow basalts and their petrology, *Geol. soc. Am. Bull.,* **82,** 537–552.

Marshall, M. & Cox, A., 1972. Magnetic changes in pillow basalt due to seafloor weathering, *J. geophys. Res.,* **77,** 6459–6469.

Nishitani, T. & Kono, M., 1983. Curie temperature and lattice constant of oxidized titanomagnetite, *Geophys. J. R. astr. Soc.,* **74,** 585–600.

Özdemir, Ö., 1987. Inversion of titanomaghemites, *Phys. Earth Planet. Inter.,* **46,** 184–196.

Özdemir, Ö. & Dunlop, D.J., 1985. An experimental study of chemical remanent magnetizations of synthetic monodomain titanomaghemites with initial thermoremanent magnetizations, *J. geophys. Res.,* **90,** 1513–1523.

Ozima, M., 1971. Characteristic Thermomagnetic curve in submarine basalts, *J. geophys. Res.,* **76,** 2051–2056.

Petersen, N. & Vali, H., 1987. Observation of shrinkage cracks in ocean floor titanomagnetites, *Phys. Earth planet. Inter.,* **46** (1–3), 197–205.

Readman, P.W. & O'Reilly, W., 1972. Magnetic properties of oxidized (cation-deficient) titanomagnetites (Fe, Ti)$_3$O$_4$, *J. Geomag. Geoelectr.,* **24,** 69–90.

Sayanagi, K. & Tamaki, K., 1992. Long term variations in magnetization intensity with crustal age in the Northeast Pacific, Atlantic, and Southeast Indian Oceans, *Geophys. Res. Lett.,* **19,** 2369–2372.

van Aken, P.A. & Liebscher, B., 2002. Quantification of ferrous/ferric ratios in minerals: new evaluation schemes of Fe L_{23} electron energy-loss near-edge spectra, *Phys. Chem. Miner.,* **29,** 188–200.

Grommé, S., Mankinen, E.A., Marshall, M. & Coe, R.S., 1979. Geomagnetic paleointensities by the Thelliers' method from submarine pillow basalts: effects of seafloor weathering, *J. geophys. Res.,* **84,** 3553–3575.

Hodych, J.P. & Matzka, J., 2004. Saturation magnetostriction and its low-

Vine, F.J. & Matthews, D.H., 1963. Magnetic anomalies over oceanic ridges, *Nature,* **199,** 947–949.

Vogt, P.R. & Johnson, G.L., 1973. Magnetic telechemistry of oceanic crust, *Nature,* **245,** 373–375.

Worm, H.U. & Banerjee, S.K., 1984. Aqueous low temperature oxidation of titanomagnetite, *Geophys. Res. Lett.,* **11,** 169–172.

Xu, W.X., Peacor, D.R., Dollase, W.A., Van der Voo, R. & Beaubouef, R., 1997. Transformation of titanomagnetite to titanomaghemite: a slow, two-step, oxidation-ordering process in MORB, *Am. Miner.,* **82,** 1101–1110.

Zhou, W.M., Peacor, D.R., Van der Voo, R. & Mansfield, J.F., 1999a. Determination of lattice parameter, oxidation state, and composition of indi-

vidual titanomagnetite/titanomaghemite grains by transmission electron microscopy, *J. geophys. Res.,* **104,** 17 689–17 702.

Zhou, W.M., Van der Voo, R. & Peacor, D.R., 1999b. Preservation of pristine titanomagnetite in older ocean-floor basalts and its significance for paleointensity studies, *Geology,* **27,** 1043–1046.

Zhou, W.M., Van der Voo, R., Peacor, D.R., Wang, D.M. & Zhang, Y.X., 2001. Low-temperature oxidation in MORB of titanomagnetite to titanomaghemite: a gradual process with implications for marine magnetic anomaly amplitudes, *J. geophys. Res.,* **106,** 6409–6421.

Zhou, W.M., Van der Voo, R., Peacor, D.R. & Zhang, Y.X., 2000. Variable Ti-content and grain size of titanomagnetite as a function of cooling rate in very young MORB, *Earth planet. Sci. Lett.,* **179,** 9–20.